ADVANCED MATERIALS
www.advmat.de

Neutrophil/Leukemia-Tropic Dual-Drug Nanomedicine Potentiates the Treatment of Acute Myeloid Leukemia

Shujing Yue, Zhenzhen Zhai, Jingnan An, Huanli Sun, Jiaying Li, Cenzhu Zhao, Yang Xu, and Zhiyuan Zhong**

Acute myeloid leukemia (AML) poses severe clinical challenges due to its heterogeneity and the scattered nature of therapeutic targets. Moreover, suboptimal drug delivery to the bone marrow, combined with the protective effects of the niche that shelters residual leukemia cells, frequently underlies chemotherapy failure and relapse. Here, a neutrophil/leukemia-tropic polymersome vincristine/volasertib dual-drug nanoformulation (NLP-Vi/Vo) is reported to selectively bind to leukemia cells and neutrophils, and to ratiometrically release clinical chemotherapeutics and a polo-like kinase 1 inhibitor, thereby potentiating the treatment of AML. NLP-Vi/Vo induces synergistic anti-AML effects by sensitizing AML to chemotherapy, and homes to bone marrow by hitchhiking on neutrophils, cooperatively depleting leukemia in both the bloodstream and bone marrow. NLP-Vi/Vo shows excellent therapeutic efficacy in malignant murine AML and human AML xenograft models. Collectively, neutrophil/leukemia-directing dual-drug nanomedicines offer a promising treatment strategy for AML.

1. Introduction

Acute myeloid leukemia (AML), characterized by the abnormal proliferation of myeloid blasts in the bone marrow and peripheral blood, is fatal to most patients.[1–3] Chemotherapy has long been the gold standard treatment, but is associated with dismal clinical efficacy and a high relapse rate as a result of serious toxic effects and drug resistance.[4–7] Recent advances in a small number of molecular targeted drugs and the integration of them with chemotherapeutics have demonstrated certain improvements in therapeutic efficacy by potentially sensitizing AML to chemotherapy, inducing synergistic effects, and/or overcoming drug resistance.[8,9] However, the clinical outcome of drug combinations remains limited by several critical challenges, including uncontrollable drug ratios in vivo and overlapping toxicities.[10] Co-loading two drugs in one nanomedicine presents an exciting approach.[11,12] For example, the clinically successful liposomal dual-drug CPX-351 (Vyxeos) ratiometrically delivers cytarabine and daunorubicin chemotherapeutics, leading to an increased response rate in AML patients compared with the free drug combination.[13,14] However, a small population of leukemia cells is often resistant to chemotherapy, which makes their complete eradication particularly difficult when chemotherapy alone is used.[15,16]

Inferior drug delivery to the bone marrow poses another critical challenge hampering leukemia depletion and causing relapse.[17,18] To address this issue, bone-targeting bisphosphonate-directed nanodelivery systems have been developed;[19,20] however, drug accumulation in the bone marrow is still limited owing to the bone marrow-blood barrier. Neutrophils, the most common type of circulating leukocyte in the body, have a short lifespan, and senescent neutrophils naturally home to the bone marrow for apoptosis.[21,22] Leveraging this advantage, neutrophils were engineered ex vivo to load single-drug nanomedicines and increase drug accumulation in the bone marrow, resulting in improved treatment of bone metastatic breast tumors and osteoporosis in mice.[23]

In this contribution, we propose a neutrophil/leukemia-tropic polymersome-based dual-drug nanoformulation (NLP-Vi/Vo) that induces synergistic anti-AML effects by ratiometrically delivering the chemotherapeutic vincristine and the polo-like kinase 1 (PLK1) inhibitor volasertib to the leukemic cells (**Figure 1**a,b). By hitchhiking on neutrophils, the polymersomes are homed to the bone marrow to potentiate the treatment of AML. Elevated PLK1 expression is frequently associated with poor prognosis and resistance to chemotherapy in diverse

S. Yue, Z. Zhai, H. Sun, Z. Zhong
State Key Laboratory of Bioinspired Interfacial Materials Science and Biomedical Polymers Laboratory
College of Chemistry
Chemical Engineering and Materials Science
Soochow University
Suzhou 215123, P. R. China
E-mail: sunhuanli@suda.edu.cn; zyzhong@suda.edu.cn

J. An, C. Zhao, Y. Xu
Jiangsu Institute of Hematology
The First Affiliated Hospital of Soochow University
Collaborative Innovation Center of Hematology
Soochow University
Suzhou 215123, P. R. China

J. Li
Department of Orthopaedic Surgery
Orthopaedic Institute
The First Affiliated Hospital
Soochow University
Suzhou 215007, P. R. China

Z. Zhong
College of Pharmaceutical Sciences
Soochow University
Suzhou 215123, P. R. China

The ORCID identification number(s) for the author(s) of this article can be found under https://doi.org/10.1002/adma.202512635

DOI: 10.1002/adma.202512635

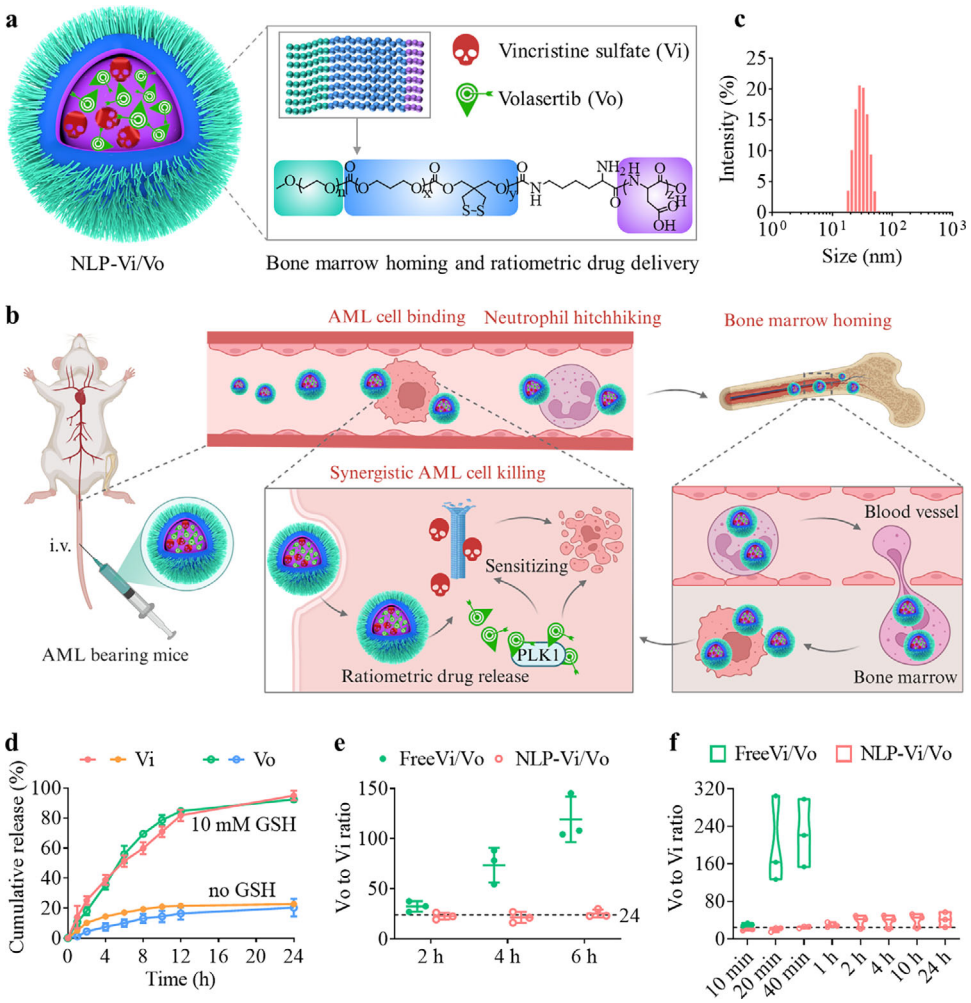

Figure 1. Preparation of a neutrophil/leukemia-tropic polymersome dual-drug nanoformulation (NLP-Vi/Vo) for enhanced treatment of AML. a) Schematic showing the composition of NLP-Vi/Vo. b) Schematic showing that NLP-Vi/Vo binds to AML cells in the blood and home to the bone marrow by hitchhiking neutrophils, thus inducing synergistic AML depletion via ratiometric release of the two drugs. c) Size distribution of NLP-Vi/$Vo_{1/24}$. d) In vitro drug release curves of NLP-Vi/Vo ($n = 3$), GSH: glutathione. e) Intracellularly released Vo/Vi ratios in NLP-Vi/$Vo_{1/24}$- or FreeVi/$Vo_{1/24}$-treated Molm-13-Luc cells ($n = 3$). f) Mouse plasma Vo/Vi ratios at different time points after intravenous injection of NLP-Vi/$Vo_{1/24}$ or FreeVi/$Vo_{1/24}$ ($n = 3$). In d–f, the data are presented as the mean ± standard deviation (SD).

malignancies, including AML.[24,25] NLP-Vi/Vo selectively binds to leukemia cells and neutrophils and sensitizes AML to chemotherapy, cooperatively eradicating leukemia cells in the bloodstream and bone marrow. The effectiveness of NLP-Vi/Vo has been demonstrated by the complete cure of three different AML models. This neutrophil/leukemia-directing polymersome dual-drug strategy presents a novel potential treatment for AML.

2. Results and Discussion

2.1. Design of NLP-Vi/Vo for Ratiometric Codelivery of Vincristine and Volasertib

Chemotherapy alone is difficult to deplete leukemia due to its heterogeneity and drug resistance. Molecular targeted drugs, such as PLK1 inhibitors, have been shown to simultaneously induce the apoptosis of cancer cells and increase their sensitivity to chemotherapy.[26,27] However, the combination of chemotherapeutics with molecular targeted drugs has achieved only limited clinical success, partly owing to their shifting drug ratios, rapid clearance, and poor bone marrow delivery. Polymersomes, featuring a bilayered structure, offer significant advantages in delivering a variety of drugs, particularly water-soluble drugs, thereby increasing their therapeutic efficacy.[28–30] Here, we developed a neutrophil/leukemia-tropic polymersome for bone marrow homing and ratiometric codelivery of Vi and Vo to potentiate the treatment of AML. Vo has been designated as an orphan drug for treating AML by the Food and Drug Administration (FDA), which can sensitize Vi, a potent chemotherapeutic drug for leukemia, and collectively induce mitotic arrest and cell apoptosis. NLP-Vi/Vo consists of a poly(ethylene glycol) outer shell, a disulfide-cross-linked polycarbonate membrane, and a negatively charged cavity, enabling ratiometric loading of Vi and Vo via electrostatic interactions. NLP-Vi/Vo formulations with different Vi/Vo mass ratios

of 1/12, 1/24, and 1/48, which were denoted as NLP-Vi/$Vo_{1/12}$, NLP-Vi/$Vo_{1/24}$, and NLP-Vi/$Vo_{1/48}$, respectively, were readily prepared by controlling the drug feed ratios. Single-drug polymersomes, NLP-Vi and NLP-Vo, were also prepared for comparison. All the nanoformulations presented consistent sizes of ≈30 nm, narrow size distributions (PDI ≤ 0.10), mildly negative zeta potentials (−4.1 – −5.5 mV), and comparable drug loading efficiencies (Figure 1c; Table S1, Supporting Information). NLP-Vi/Vo, featuring a spherical vesicular structure, exhibited remarkable stability against dilution, 10% fetal bovine serum (FBS), or 300 days of storage at 4 °C (Figures S1 and S2, Supporting Information). The exposure of NLP-Vi/Vo to 10 mM GSH, which mimics that inside cancer cells,[31] triggered the rapid and ratiometric release of Vi and Vo (Figure 1d). Moreover, NLP-Vi/$Vo_{1/24}$ ratiometrically released Vi and Vo in AML cells, contrasting sharply to the free drug combination (FreeVi/$Vo_{1/24}$), with a drug ratio deviating to 1/145 (Figure 1e). Additionally, the amount of intracellularly released Vi or Vo from NLP-Vi/Vo was consistently higher than that from FreeVi/Vo (Figure S3, Supporting Information). After intravenous injection into BALB/c mice, NLP-Vi/Vo maintained a nearly constant Vi/Vo ratio in the blood within 24 h, whereas the Vi/Vo ratio of FreeVi/Vo shifted to 1/224 after only 40 min (Figure 1f; Figure S4, Supporting Information). The ratiometric delivery of two drugs is essential for achieving synergistic antitumor effects in vivo.[32]

2.2. In vivo AML Binding, Neutrophil Hitchhiking, and Bone Marrow Homing of NLP-Vi/Vo

To evaluate the AML selectivity of NLP-Vi/Vo, Cy5-labeled polymersomes (NLP-Cy5) were intravenously injected into orthotopic Molm-13-Luc AML-bearing mice, and peripheral blood was collected for analysis. As shown in **Figure 2**a, NLP-Cy5 selectively and rapidly bound to circulating AML cells, resulting in significantly higher Cy5 intensity than that of normal peripheral blood cells. We then determined the type and population of normal peripheral blood cells associated with NLP-Cy5 in normal BALB/c mice. After intravenous injection, NLP-Cy5 quickly bound to leukocytes in the blood, and 98.4% of the Cy5-positive leukocytes were neutrophils at 1 h (Figure 2b–d; Figure S5, Supporting Information), supporting the exceptional neutrophil hitchhiking capability of NLP-Vi/Vo.

Inspired by the neutrophil hitchhiking effects of NLP-Cy5, we further investigated its bone marrow homing and AML selectivity in different tissues using orthotopic Molm-13-Luc AML-bearing mice. NLP-Cy5 effectively accumulated in the forelimbs, hindlimbs, and other leukemia-infiltrated organs, including the liver, lung, and kidney, at 4 h after injection (Figure 2e). Rapid bone marrow homing most likely stems from the NLPs associated with the circulating population of senescent neutrophils ($CXCR4^{high}CD62L^{low}$) (Figure S6, Supporting Information), which are constitutively present in mice and constitute ≈55% of blood neutrophils at peak times.[33,34] More importantly, NLP-Cy5 enriched in different tissues presented high selectivity for AML cells compared with normal cells (Figure 2f). Consistently, NLP-Vi/Vo significantly increased drug accumulation in the bone marrow by 7-fold compared with FreeVi/Vo (Figure 2g). Furthermore, partial depletion of neutrophils via intraperitoneal injection of anti-Ly6G antibody[35,36] significantly reduced the accumulation of NLP-Cy5 in the forelimbs and hindlimbs (Figure 2h,i), indicating the important role of neutrophils in navigating NLP-Vi/Vo to the bone marrow.

2.3. NLP-Vi/Vo Synergistically Inhibits AML Cells

The potential synergies of NLP-Vi/Vo in vitro were first investigated via cell viability assays using three AML cell lines (MV-4-11, Molm-13-Luc, and WEHI-3). In MV-4-11 cells, NLP-Vi/Vo with different Vi/Vo mass ratios of 1/12, 1/24, and 1/48 exhibited strong synergy, with combination indices (CIs) as low as 0.21–0.25 (Table S2, Supporting Information). For example, NLP-Vi/$Vo_{1/24}$ presented a half-maximal inhibitory concentration (IC_{50}) of 0.05 ng mL^{-1} for Vi and 1.3 ng mL^{-1} for Vo, which were 29- and 6-fold lower than those of NLP-Vi and NLP-Vo, respectively (**Figure 3**a). Moreover, NLP-Vi/$Vo_{1/24}$ was 6-fold more potent than FreeVi/$Vo_{1/24}$, which is consistent with its ability to maintain a stable intracellular drug ratio and achieve higher intracellular drug contents. A similar synergistic effect of NLP-Vi/Vo was also observed in Molm-13-Luc and WEHI-3 cells (Figure 3b; Figure S7, Supporting Information). Importantly, NLP-Vi/$Vo_{1/24}$ was nontoxic to normal mouse T cells even at a high Vo concentration of 2.4 μg mL^{-1} (Figure S8a, Supporting Information). The blank polymersomes (NLP) exhibited no discernible toxicity across three distinct AML cell lines (Figure S8b, Supporting Information).

As Vi and Vo are recognized for their capacity to induce cell cycle arrest and trigger apoptosis,[27,37] we assessed the potential synergy of NLP-Vi/Vo in enhancing G2/M arrest and apoptosis via flow cytometry. NLP-Vi/Vo sharply increased the percentage of three different AML cell lines in the G2/M phase (Figure 3c; Figure S9, Supporting Information). As a result, we observed a marked increase in apoptosis via the mitochondrial pathway in cells treated with NLP-Vi/Vo compared with those treated with control formulations (Figure 3d,e; Figures S10 and S11, Supporting Information). The synergistic proapoptotic ability of NLP-Vi/Vo was further observed in primary AML cells isolated from eight patients, with an apoptosis rate as high as ≈90% (Figure 3f). Additionally, NLP-Vi/Vo treatment most significantly reduced the protein expression of PLK1 as well as B-cell lymphoma 2 (BCL-2) and myeloid cell leukemia 1 (MCL-1) (Figure 3g), two key antiapoptotic proteins that regulate mitochondrial apoptosis.[38] Collectively, these data indicate a potent synergistic effect of NLP-Vi/Vo in inducing cell cycle arrest, causing cell apoptosis, and suppressing AML proliferation.

2.4. RNA-Seq Analysis of the Synergistic Mechanism of NLP-Vi/Vo

Inspired by the strong synergistic anti-AML effect of NLP-Vi/Vo, we further investigated the underlying mechanism via RNA-seq. Compared with PBS treatment, treatment with different formulations significantly altered the gene expression of Molm-13-Luc cells (**Figure 4**a). Additionally, genes in cells treated with NLP-Vi/Vo were also differentially regulated compared with those in cells treated with NLP-Vi, NLP-Vo, or FreeVi/Vo (Figure S12, Supporting Information). The pathway enrichment of the regulated

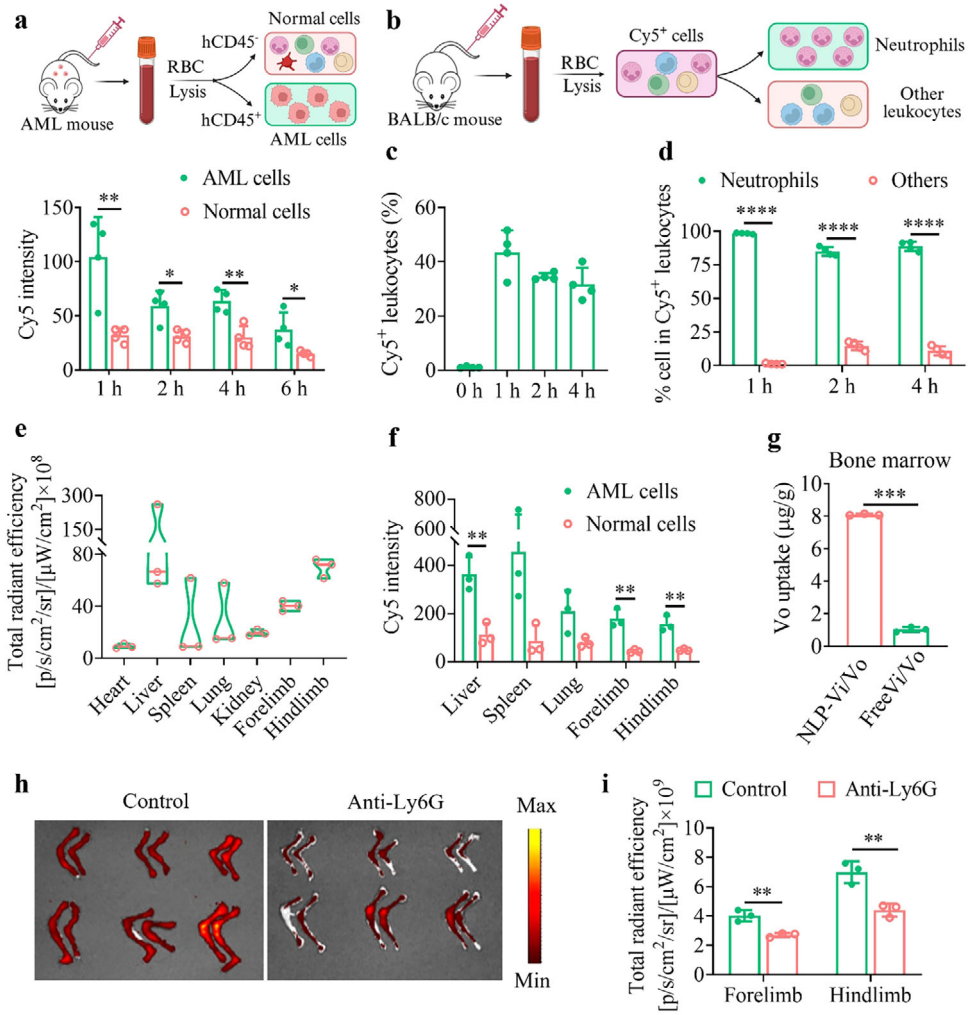

Figure 2. In vivo AML selectivity, neutrophil hitchhiking, and bone marrow homing of NLP-Vi/Vo. a) Cy5 fluorescence intensity of AML cells and normal cells in the peripheral blood after intravenous injection of NLP-Cy5 in orthotopic Molm-13-Luc AML-bearing mice ($n = 4$). b) Schematic of the sorting of $Cy5^+$ cells, as well as neutrophils and other leukocytes in the blood of BALB/c mice. c) The percentage of $Cy5^+$ cells in leukocytes in the peripheral blood at different times after intravenous injection of NLP-Cy5 into BALB/c mice ($n = 4$). d) Percentages of neutrophils and other $Cy5^+$ leukocytes in (c) ($n = 4$). e) Quantitative analysis of Cy5 fluorescence in various ex vivo imaged tissues at 4 h post-injection of NLP-Cy5 in orthotopic Molm-13-Luc AML-bearing mice ($n = 3$). f) Cy5 fluorescence intensity of AML cells and normal cells in different tissues in (e). g) Vo content in the hindlimbs of Molm-13-Luc AML-bearing mice at 6 h after intravenous injection of NLP-Vi/$Vo_{1/24}$ or FreeVi/$Vo_{1/24}$ ($n = 3$). h) Ex vivo fluorescence images of forelimbs and hindlimbs isolated from Molm-13-Luc AML-bearing mice or those treated with anti-Ly6G antibody to deplete neutrophils at 4 h post-injection of NLP-Cy5 ($n = 3$). i) Quantitative fluorescence analysis of (h) ($n = 3$). Statistical significance was analyzed by an unpaired Student's *t*-test for (a,d,f,g,i). $^*p < 0.05$, $^{**}p < 0.01$, $^{***}p < 0.001$, $^{****}p < 0.0001$. The data are presented as the mean ± SD for (a, c-g, i).

genes was further assessed via Kyoto Encyclopedia of Genes and Genomes (KEGG) analysis. As shown in Figure 4b, the downregulated genes observed between different treatments and PBS were strongly enriched in the cell cycle and DNA replication pathways, with NLP-Vi/Vo treatment inducing the most pronounced enrichment in the cell cycle pathway. Notably, unlike single drug formulations and FreeVi/Vo controls, NLP-Vi/Vo uniquely induced the activation of necroptosis, ferroptosis, apoptosis, and Toll-like receptor signaling pathways as well as the inhibition of microRNAs in cancer and the transforming growth factor-β (TGF-β) pathways. Emerging evidence indicates that ferroptosis activation and TGF-β inhibition can reverse drug resistance in cancer,[39–42] which may contribute to the strong synergistic effects of NLP-Vi/Vo. Gene set enrichment analysis (GSEA) of the KEGG datasets further demonstrated the significant downregulation of the cell cycle and TGF-β pathways by NLP-Vi/Vo (Figure 4c). Gene Ontology (GO) analysis additionally revealed that NLP-Vi/Vo treatment downregulated genes related to the cell cycle phase transition and mitosis compared with the NLP-Vi and NLP-Vo controls (Figure S13, Supporting Information). Moreover, enriched GSEA expression was observed in the p53 signaling pathway after NLP-Vi/Vo treatment, which is in contrast to FreeVi/Vo with a negative regulation (Figure 4d). This is likely due to the increased intracellular delivery of drugs by NLP-Vi/Vo. The gene heatmaps revealed that NLP-Vi/Vo significantly regulated the expression of genes related to the cell

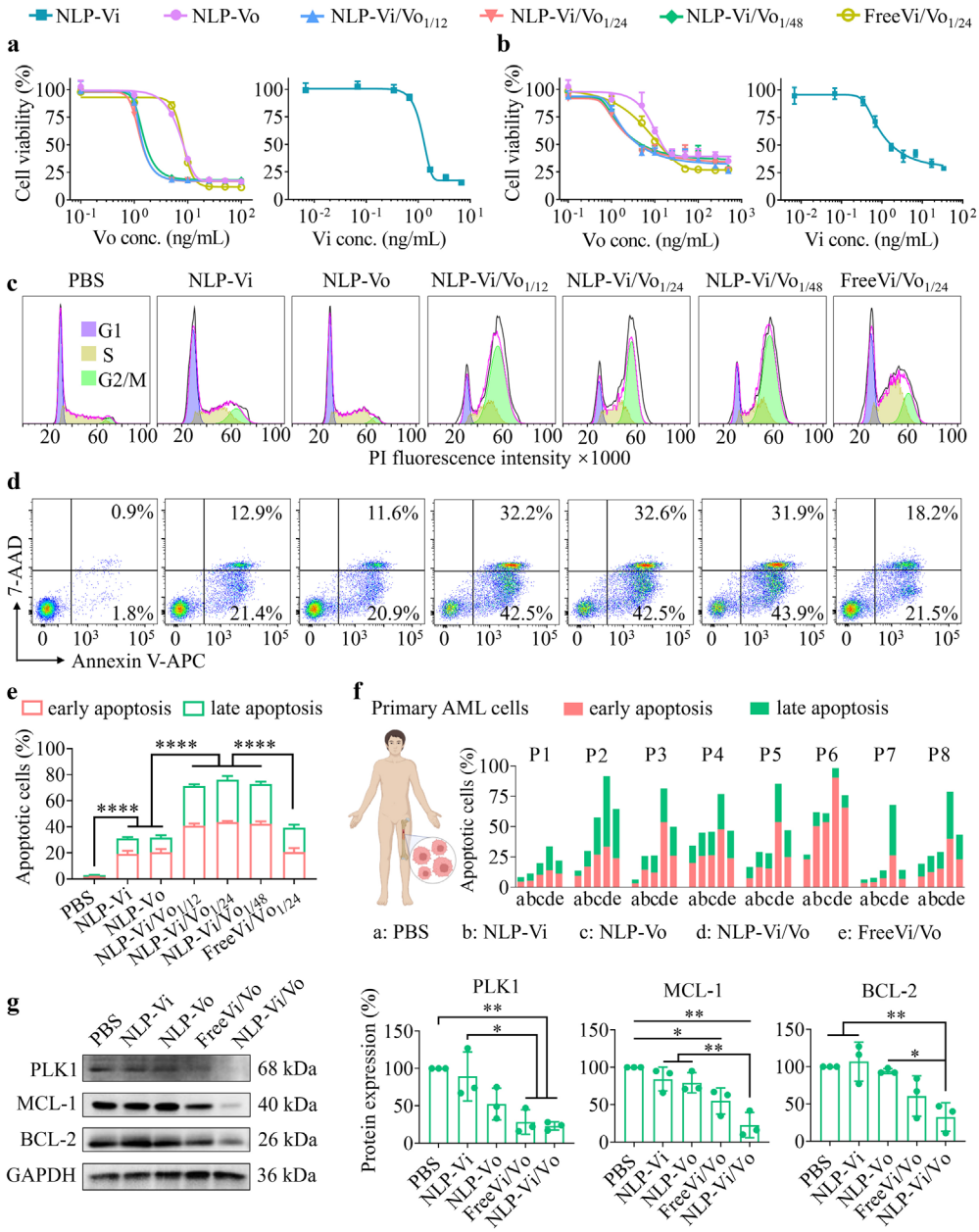

Figure 3. Synergistic antileukemic activity of NLP-Vi/Vo in vitro. a,b) Anti-AML activity of NLP-Vi/Vo with different Vi/Vo ratios, NLP-Vi, NLP-Vo, and FreeVi/Vo$_{1/24}$ in MV-4-11 (a) and Molm-13-Luc cells (b) ($n = 6$). c) Representative cell cycle analysis of Molm-13-Luc cells following different treatments via propidium iodide (PI) staining. d) Representative apoptosis pattern of Molm-13-Luc cells following different treatments and e) quantitative analysis ($n = 3$). f) Apoptosis analysis of CD33$^+$ AML blasts isolated from AML patients after incubation with PBS, NLP-Vi, NLP-Vo, NLP-Vi/Vo, or FreeVi/Vo (Vi/Vo = 1/24). g) Representative western blot images and grayscale quantifications of PLK1, BCL-2, MCL-1 and GAPDH proteins in Molm-13-Luc cells following different treatments ($n = 3$). $^*p < 0.05$, $^{**}p < 0.01$, $^{****}p < 0.0001$. The data are presented as the mean ± SD for (a,b,e,g).

cycle (CDC14B, WEE1, MYC, E2F5, etc.), TGF-β (MYC, E2F5, INHBE, BMP2, INHBC, RHOA), apoptosis (BCL-2, BAX, etc.), and ferroptosis (CYBB, HMOX1, STEAP3, SLC3A2, etc.) (Figure 4e). Western blot analysis further showed that NLP-Vi/Vo treatment significantly elevated cleaved caspase-3 and Bax—hallmarks of apoptosis—together with the CDK inhibitor p21, while concomitantly reducing total CDK1 and its inhibitory phosphorylation (pCDK1), confirming G2/M blockade and concurrent apoptotic induction (Figure S14, Supporting Information).

2.5. NLP-Vi/Vo-Mediated Depletion of Leukemia Cells In vivo

The synergistic in vivo anti-AML efficacy of NLP-Vi/Vo at different Vi/Vo dosages of 0.25/3, 0.25/6, and 0.125/6 mg kg^{-1}, which were denoted as NLP-Vi/Vo$_{0.25/3}$, NLP-Vi/Vo$_{0.25/6}$, and NLP-Vi/Vo$_{0.125/6}$, respectively, was first assessed in an orthotopic FMS-like tyrosine kinase 3-internal tandem duplication (FLT3-ITD) mutant Molm-13-Luc AML model (**Figure** 5a). FLT3-ITD is the most prevalent mutation in AML and is strongly

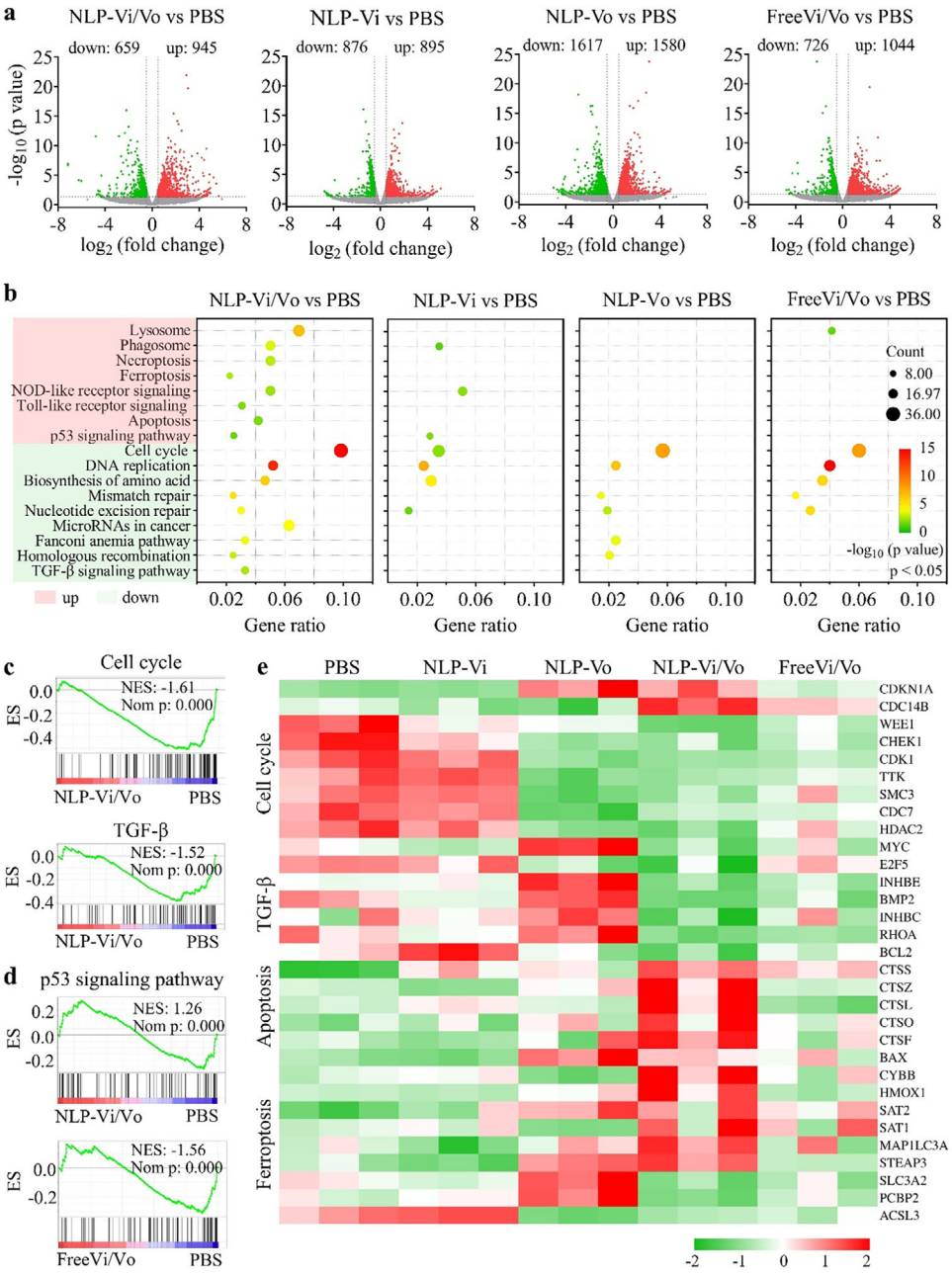

Figure 4. RNA-seq analysis of Molm-13-Luc cells after different treatments ($n = 3$). a) Volcano plots depicting genes differentially expressed between cells treated with NLP-Vi/Vo, NLP-Vi, NLP-Vo, or FreeVi/Vo and those treated with PBS. Genes exhibiting a p-value < 0.05 and an absolute log2 (fold change) > 0.5 were recognized as differentially expressed genes (DEGs). b) Significantly enriched KEGG pathways of genes differentially expressed in cells after treatment with NLP-Vi/Vo, NLP-Vi, NLP-Vo, or FreeVi/Vo compared to PBS-treated cells. c) GSEA plots showing the downregulated cell cycle and TGF-β pathways after treatment with NLP-Vi/Vo. ES: enrichment score; NES: normalized enrichment score; Nom p: normalized p value. d) GSEA plots showing the regulation of the p53 signaling pathway after treatment with NLP-Vi/Vo or FreeVi/Vo. e) Heatmaps of DEGs related to the cell cycle, TGF-β, apoptosis, and ferroptosis.

associated with poor clinical outcomes.[43] NLP-Vi, NLP-Vo, FreeVi/Vo (Vi: 0.25 mg kg^{-1}, Vo: 6 mg kg^{-1}), and PBS served as controls. Leukemia growth was monitored by bioluminescence signals from Molm-13-Luc cells. Four injections of NLP-Vi/Vo strongly inhibited the proliferation of leukemia cells, and NLP-Vi/Vo$_{0.25/6}$ presented the most effective leukemia inhibition, with no detectable bioluminescence signals in any of the mice (Figure 5b,c). However, treatment with single drug nanoformulations (NLP-Vi, NLP-Vo) or FreeVi/Vo only retarded leukemia progression to a certain extent. As a result, NLP-Vi/Vo significantly outperformed the other control formulations in prolonging survival, with 100% of the mice in the NLP-Vi/Vo$_{0.25/6}$ group surviving for at least 180 days (Figure 5d). The mice in all treatment cohorts maintained stable weights (Figure 5e). Moreover,

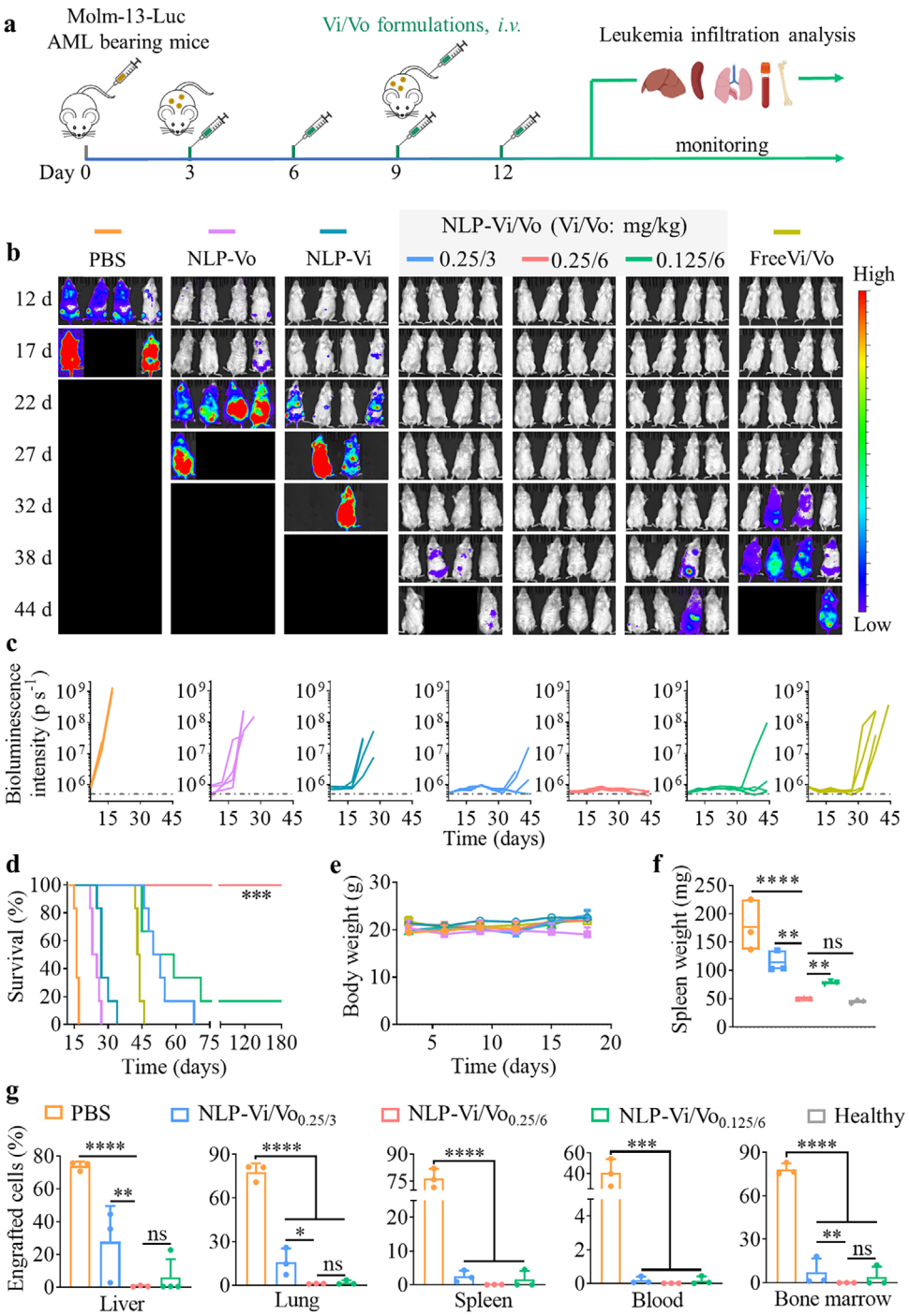

Figure 5. NLP-Vi/Vo-mediated depletion of leukemia cells in the orthotopic Molm-13-Luc AML model. a) Treatment and monitoring scheme. b) Bioluminescence images showing leukemia progression in mice treated with PBS, NLP-Vo, NLP-Vi, NLP-Vi/$Vo_{0.25/3}$, NLP-Vi/$Vo_{0.25/6}$, NLP-Vi/$Vo_{0.125/6}$, and FreeVi/Vo. c) Analysis of bioluminescence intensity across regions of interest within the whole body of each mouse from different groups. d) Survival curves of the mice in different treatment groups ($n = 6$). Statistical significance was calculated via the log-rank test: NLP-Vi/$Vo_{0.25/6}$ versus FreeVi/Vo, NLP-Vi, NLP-Vo, and PBS, $^{***}p < 0.001$. e) Weight variations in mice that received different treatments ($n = 6$). f), Spleen weight after treatment with NLP-Vi/Vo or PBS ($n = 3$). Healthy mice were used as controls. g) Percentages of AML cells in the liver, lung, spleen, peripheral blood, and bone marrow ($n = 3$). Statistical significance was analyzed by one-way ANOVA for (f, g), $^{*}p < 0.05$, $^{**}p < 0.01$, $^{***}p < 0.001$, $^{****}p < 0.0001$. The data are presented as the mean ± SD for (e-g).

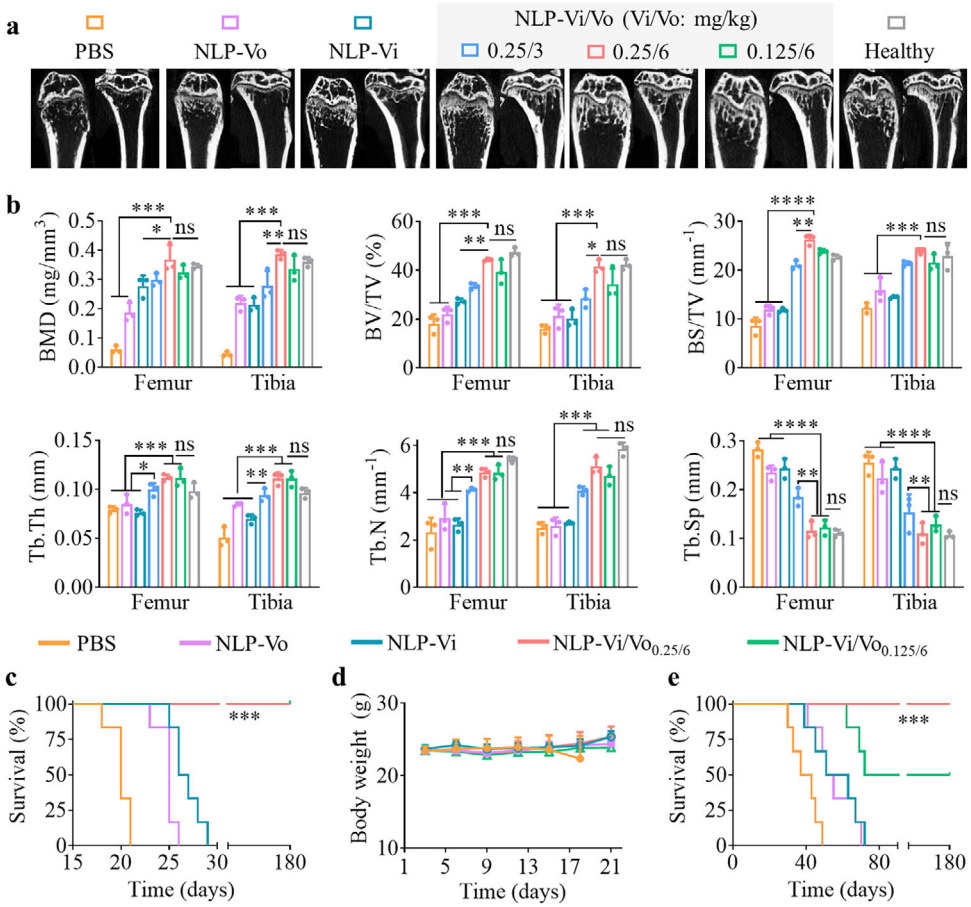

Figure 6. Leukemia infiltration analysis and synergistic anti-AML effects in different AML models. a) Representative micro-CT images of femurs and tibias isolated from mice in different groups. The experiments were repeated three times. b) Quantitative parameter analysis of the femurs and tibias. BMD: bone mineral density; BV/TV: bone volume fraction; BS/TV: bone surface area/bone volume; Tb.Th: trabecular thickness; Tb.N: trabecular number; Tb.Sp: trabecular separation ($n = 3$). Statistical significance was analyzed by one-way ANOVA, $^{*}p < 0.05$, $^{**}p < 0.01$, $^{***}p < 0.001$, $^{****}p < 0.0001$. c) Survival curves and d) body weight changes of orthotopic MV-4-11-bearing mice receiving different formulations ($n = 6$). e) Survival curves of orthotopic WEHI-3 AML-bearing mice receiving different formulations ($n = 6$). The data are presented as the mean ± SD for (b,d). Statistical significance was analyzed via the log-rank test for (c,e) (NLP-Vi/$Vo_{0.25/6}$ versus NLP-Vi, NLP-Vo, or PBS, $^{***}p < 0.001$).

a single injection of NLP-Vi/Vo at 4-fold higher dosages (Vi/Vo: 1/12, 1/24, and 0.5/24 mg kg^{-1}) induced negligible changes in the blood routine and biochemical parameters of the mice, resulting in a survival rate of 100% (Figure S15, Supporting Information).

AML cells are known to abnormally proliferate in the bone marrow and infiltrate extramedullary tissues, leading to characteristic clinical symptoms such as splenomegaly and bone marrow failure.[44,45] NLP-Vi/Vo treatment significantly inhibited splenomegaly in the mice, for which the spleen weight was similar to that observed in healthy mice and ca. 1/3 the weight of the spleen from the PBS group (Figure 5f). Additional evidence was provided by the complete suppression of leukemia infiltration in various tissues of mice in the NLP-Vi/$Vo_{0.25/6}$ group (Figure 5g; Figure S16, Supporting Information). Consistently, the bone marrow failure in the control groups, characterized by an apparent reduction in hematopoietic cells[46,47] was completely relieved in the NLP-Vi/$Vo_{0.25/6}$ group (Figure S17, Supporting Information). The expansion of leukemia cells in the bone marrow can activate osteoclasts and regulate osteolytic activities, resulting in osteopenia.[48] Tartrate-resistant acid phosphatase (TRAP)-stained images revealed that the number of osteoclasts in mice treated with NLP-Vi/$Vo_{0.25/6}$ decreased to a level similar to that in healthy mice (Figure S18, Supporting Information). Micro-CT was then utilized to assess the bone structure of the hindlimbs. NLP-Vi/$Vo_{0.25/6}$ treatment completely prevented bone loss in the mice, resulting in a normal bone structure and related parameters akin to those observed in healthy mice, outperforming NLP-Vi and NLP-Vo (**Figure 6**a,b).

To further corroborate the synergistic anti-AML effect of NLP-Vi/Vo, we established FLT3-ITD mutant human MV-4-11 as well as syngeneic, FLT3 wild-type, lysine methyltransferase 2A (KMT2A) rearranged WEHI-3 AML models. The mice were intravenously injected with PBS, NLP-Vi, NLP-Vo, or NLP-Vi/Vo (Vi/Vo: 0.25/6 and 0.125/6 mg kg^{-1}) under the same regimen as the Molm-13-Luc AML model. In the MV-4-11 model, NLP-Vi/Vo treatment completely eradicated leukemia cells, resulting in 100% survival of the mice after 180 days, whereas no mice in the other control groups survived beyond 30 days (Figure 6c). Similar results were also observed in the syngeneic WEHI-3

model, in which 100% of the mice survived after treatment with NLP-Vi/$Vo_{0.25/6}$ (Figure 6e). Stable body weights were observed for the mice in all the groups (Figure 6d; Figure S19, Supporting Information). Taken together, these findings demonstrated the applicability of NLP-Vi/Vo in curing FLT3-ITD mutant and/or KMT2A rearranged AML models and the superiority of ratiometrically codelivering Vi/Vo in leukemia treatment.

3. Conclusion

AML patients continue to face high mortality rates due to limited targeted treatments and difficulty in eradicating leukemia cells in the bone marrow. In this work, we report a neutrophil/leukemia-affinitive polymersome vincristine/volasertib dual-drug nanoformulation (NLP-Vi/Vo) to address this challenge. NLP-Vi/Vo with superb stability ratiometrically delivered chemotherapeutics and PLK1 inhibitors to leukemia cells, resulting in a strong synergistic anti-AML effect via the regulation of diverse pathways. NLP-Vi/Vo was able to selectively bind to AML cells and home to the bone marrow by hitchhiking neutrophils, completely depleting leukemia cells in mice and curing different models. Overall, these neutrophil/leukemia-directing dual-drug nanomedicines significantly potentiate AML treatment via neutrophil-mediated bone marrow homing and the ratiometric delivery of chemotherapeutics and molecular targeted agents. The greater abundance of circulating neutrophils in humans might afford increased hitchhiking capacity; however, fundamental interspecific differences mandate comprehensive humanized assays to ensure reliable clinical translation. Moreover, a complete CMC dossier for both the polymeric excipients and the final NLP-Vi/Vo formulation, underpinned by continuous, scalable manufacturing and rigorous quality-control strategies, is essential to expedite clinical development.

4. Experimental Section

Antibodies: PE anti-human-CD33 antibody (Cat: 366606), APC-Cy7 Zombie NIR fixable viability kit (Cat: 423106), PE-Cy7 anti-mouse Ly6G/Ly6C (Gr-1) antibody (Cat: 108416), FITC anti-mouse/human CD11b antibody (Cat: 101206), FITC or PE anti-human CD45 antibody (Cat: 304006, 304008), PE-Cy5 anti-mouse Ly6G antibody (Cat: 127671), PE anti-mouse CXCR4 antibody (Cat: 146505), and PE-Cy7 anti-mouse CD62L antibody (Cat: 104418) were purchased from BioLegend. InVivoMAB anti-mouse Ly6G antibody (Cat: BE0075) was obtained from BioXcell. CDK1 and BCL-2 antibodies were purchased from Proteintech. MCL-1, cleaved caspase-3, p21, and pCDK1(Tyr15) antibodies were purchased from Cell Signaling Technology. Bax, PLK1, and GAPDH antibodies were purchased from Affinity Biosciences, HUABIO, and Abcam, respectively. Goat anti-rabbit antibody was purchased from Servicebio.

Preparation of NLP-Vi/Vo: NLP-Vi/Vo was fabricated via self-assembly of poly(ethylene glycol)-*b*-poly(trimethylene carbonate-*co*-dithiolane trimethylene carbonate)-*b*-poly(aspartic acid) (PEG-P(TMC-DTC)-PAsp, 5.0-(15.0–2.0)-1.29 kg mol^{-1}), synthesized with a similar protocol as the previous report.[49] Vi and Vo with different feeding mass ratios of 1:8, 1:16, and 1:32 were simultaneously loaded via electrostatic interactions. Taking 1:16 as an example, a mixture of PEG-P(TMC-DTC)-PAsp (40 mg mL^{-1}, 4.3 mL) and Vo (20 mg mL^{-1}, 1.75 mL) dissolved in dimethyl sulfoxide (DMSO) was slowly injected into 38 mL of HEPES (5 mM, pH 6.8) containing 2.2 mg of Vi under stirring. Following an overnight incubation, the solution was transferred into a dialysis bag (MWCO: 3.5 kDa) and dialyzed against HEPES (5 mM, pH 7.4) for 8 h to remove unloaded drugs and DMSO. The polymersomes obtained were denoted as NLP-Vi/Vo. The quantification of encapsulated Vi and Vo was described in Supplementary Methods. Vi or Vo-loaded single-drug polymersomes were fabricated as controls, as described for NLP-Vi/Vo, but only one drug was added during the assembly process. The obtained polymersomes were denoted as NLP-Vi and NLP-Vo, respectively.

Primary AML Cells and Animals: Primary human AML cells were isolated from bone marrow aspirates obtained from AML patients at Jiangsu Institute of Hematology, the First Affiliated Hospital of Soochow University (Suzhou, China), using Ficoll-Hypaque density centrifugation followed by fluorescent cell sorting. Informed consent was signed by patients and donors according to the guidelines given by the ethical committee of the First Affiliated Hospital of Soochow University (approval no. 2017169–2). The primary AML cells were cultured in IMDM (Gibco) supplemented with 10% FBS, 1% penicillin and streptomycin, 25 ng mL^{-1} interleukin-6, 5 ng mL^{-1} interleukin-3, 50 ng mL^{-1} stem cell factor, and 10 ng mL^{-1} FLT3 ligand.

Female BALB/c mice (6-7 weeks) and Kunming mice (6-7 weeks, half male, half female) were obtained from Beijing Vital River. Female B-NDG mice (6-7 weeks) were purchased from Biocytogen. All the animal experiments were approved by the Animal Care and Use Committee of Soochow University (Suzhou, China), and all protocols of animal studies conformed to the Guide for the Care and Use of Laboratory Animals (approval no. SYXK 2021–0065).

In vitro Synergistic Anti-AML Effects of NLP-Vi/Vo: The synergistic effects of NLP-Vi/Vo with different Vi/Vo ratios were evaluated in Molm-13-Luc, MV-4-11, and WEHI-3 AML cells using a cell counting kit-8 (CCK-8). The cells in 96-well plates (2×10^4 cells per well) were incubated with NLP-Vi/$Vo_{1/12}$, NLP-Vi/$Vo_{1/24}$, NLP-Vi/$Vo_{1/48}$, NLP-Vi, NLP-Vo, or FreeVi/$Vo_{1/24}$ for 48 h. For the NLP-Vi group, the Vi concentration was 0.007–6.8 ng mL^{-1} for the MV-4-11 cells and 0.007–34 ng mL^{-1} for the Molm-13-Luc and WEHI-3 cells. For all other formulations, the Vo concentration was 0.1–100 ng mL^{-1} for the MV-4-11 cells and 0.1–500 ng mL^{-1} for the Molm-13-Luc and WEHI-3 cells. After incubation, CCK-8 solution was added (10 µL each) and incubated for an additional 3 h. The absorbance at 450 nm was determined using a microplate reader ($n = 6$). The synergy between Vi and Vo was evaluated by determining the CI value using the subsequent formula:

$$CI = \frac{IC_{50} \text{ of Vi in combination}}{IC_{50} \text{ of Vi alone}} + \frac{IC_{50} \text{ of Vo in combination}}{IC_{50} \text{ of Vo alone}} \quad (1)$$

CI < 1, CI = 1, and CI > 1 indicate synergistic, additive, and antagonistic effects, respectively.

The cytotoxicity of NLP-Vi/$Vo_{1/24}$ against normal mouse T cells, as well as that of the blank NLP toward Molm-13-Luc, MV-4-11, and WEHI-3 AML cells, was assessed in the same manner.

In vivo Neutrophil Hitchhiking, Biodistribution, and AML Selectivity: The binding of NLP-Cy5 to neutrophils and other normal cells in the blood was evaluated in BALB/c mice. 150 µL of Cy5-labeled polymersomes (NLP-Cy5) was intravenously injected into the mice, and 150 µL of blood was collected orbitally at 0, 1, 2, and 4 h after injection ($n = 3$). After erythrocyte lysis, APC-Cy7 Zombie NIR was added for dead cell staining, and the samples were blocked for 10 min with an anti-CD16/32 antibody. Then, FITC anti-mouse/human CD11b and PE-Cy7 anti-mouse Gr-1 antibodies were used to stain the neutrophils, which were then detected via flow cytometry. To prove the role of neutrophil hitchhiking in the bone marrow homing of NLP-Cy5, mice bearing orthotopic Molm-13-Luc AML were intraperitoneally injected with an anti-mouse Ly6G antibody[35,36] on days 15 and 17 after model establishment to partially deplete the neutrophils. Another three mice without treatment were used as controls. On day 18, the mice were intravenously injected with NLP-Cy5 (0.2 µg Cy5 for each mouse). 4 h post-injection, blood samples were collected from the orbit to analyze the percentage of neutrophils by CD11b/Gr-1 staining. The major organs, along with leg bones, were harvested for ex vivo fluorescence imaging. After imaging, the liver, spleen, lung, and leg bones were homogenized and stained with a PE anti-human CD45 antibody to analyze the AML selectivity of NLP-Cy5 via flow cytometry.

The Performance of NLP-Vi/Vo in Different AML Models: The synergistic anti-AML performance of NLP-Vi/Vo was first evaluated in mice bearing orthotopic Molm-13-Luc AML. On day 3 after model establishment, the mice were divided randomly into 7 groups ($n = 13$), and treatment was initiated with tail vein injections every 3 days for four times. The treatments included NLP-Vi/Vo at different Vi/Vo dosages of 0.25/3, 0.25/6, and 0.125/6 mg kg^{-1}, FreeVi/Vo (0.25/6 mg kg^{-1}), NLP-Vi (Vi: 0.25 mg kg^{-1}), NLP-Vo (Vo: 6 mg kg^{-1}), and PBS. For each experimental group, six mice were employed to monitor survival and body weight changes, four mice were utilized to monitor leukemia growth through bioluminescence imaging, and three mice were used to monitor leukemia infiltration in different tissues and to conduct micro-computed tomography (micro-CT) and histological analysis. To enable bioluminescence imaging, each mouse was intraperitoneally injected with D-Luciferin (150 µL, 75 mg kg^{-1}), and bioluminescence images were acquired 10 min later. The weight of mice was recorded every 3 days. On day 43, three mice in each NLP-Vi/Vo-treated group were sacrificed to collect peripheral blood, major organs, and hindlimbs for leukemia burden, histological, and micro-CT analyses. Samples from the PBS, NLP-Vi, and NLP-Vo groups were collected at the endpoint for comparison. The spleen of each sacrificed mouse was weighed. To systematically evaluate the synergistic anti-AML activity of NLP-Vi/Vo, orthotopic human MV-4-11 and mouse WEHI-3 models were further established through tail vein injection of MV-4-11 cells (5×10^5) into each female B-NDG mouse and WEHI-3 cells (5×10^6) into each female BALB/c mouse. The mice were treated with PBS, NLP-Vi (Vi: 0.25 mg kg^{-1}), NLP-Vo (Vo: 6 mg kg^{-1}) or NLP-Vi/Vo (Vi/Vo: 0.25/6 and 0.125/6 mg kg^{-1}) under a similar schedule and drug dosage to that of the Molm-13-Luc model ($n = 6$).

Statistical Analysis: The data were presented as the mean ± SD. Statistical analysis was performed via GraphPad Prism 8 software. Two-tailed Student *t*-tests were used for comparisons between two groups. One-way analysis of variance (ANOVA) with Tukey's post hoc test was used for comparisons within three or more groups. A log-rank test (Mantel-Cox) was used to compare the survival of the mice between two groups. $^{*}p < 0.05$, $^{**}p < 0.01$, $^{***}p < 0.001$, $^{****}p < 0.0001$.

Supporting Information

Supporting Information is available from the Wiley Online Library or from the author.

Acknowledgements

S.Y. and Z.Z. contributed equally to this work. This work was supported by the National Natural Science Foundation of China (52273251, 52473264, and 52233007). The authors thank Prof. Yizhen Li from the Children's Hospital of Soochow University for the insightful discussions. The schemes in the figures were created with BioRender.com.

Conflict of Interest

The authors declare no conflict of interest.

Data Availability Statement

The data that support the findings of this study are available from the corresponding author upon reasonable request.

Keywords

hematological malignancy, neutrophil hitchhiking, polymersomes, ratiometric delivery, synergistic therapy

Received: July 2, 2025
Revised: October 9, 2025
Published online:

[1] C. D. DiNardo, H. P. Erba, S. D. Freeman, A. H. Wei, *Lancet* **2023**, *401*, 2073.
[2] J. Schaefer, S. Cassidy, R. M. Webster, *Nat. Rev. Drug Discovery* **2020**, *19*, 233.
[3] V. Trujillo-Alonso, E. C. Pratt, H. Zong, A. Lara-Martinez, C. Kaittanis, M. O. Rabie, V. Longo, M. W. Becker, G. J. Roboz, J. Grimm, M. L. Guzman, *Nat. Nanotechnol.* **2019**, *14*, 616.
[4] H. M. Kantarjian, C. D. DiNardo, T. M. Kadia, N. G. Daver, J. K. Altman, E. M. Stein, E. Jabbour, C. A. Schiffer, A. Lang, F. Ravandi, *CA Cancer J. Clin.* **2025**, *75*, 46.
[5] C. Sheridan, *Nat. Biotechnol.* **2017**, *35*, 696.
[6] S. J. Yue, J. N. An, Y. F. Zhang, J. Y. Li, C. Z. Zhao, J. Y. Liu, L. L. Liang, H. L. Sun, Y. Xu, Z. Y. Zhong, *Adv. Mater.* **2023**, *35*, 2209984.
[7] Q. Hu, W. Sun, J. Wang, H. Ruan, X. Zhang, Y. Ye, S. Shen, C. Wang, W. Lu, K. Cheng, G. Dotti, J. F. Zeidner, J. Wang, Z. Gu, *Nat. Biomed. Eng.* **2018**, *2*, 831.
[8] R. S. Bhansali, K. W. Pratz, C. Lai, *J. Hematol. Oncol.* **2023**, *16*, 29.
[9] H. Döhner, A. H. Wei, B. Löwenberg, *Nat. Rev. Clin. Oncol.* **2021**, *18*, 577.
[10] R. X. Zhang, H. L. Wong, H. Y. Xue, J. Y. Eoh, X. Y. Wu, *J. Controlled Release* **2016**, *240*, 489.
[11] A. Detappe, H. V. T. Nguyen, Y. Jiang, M. P. Agius, W. Wang, C. Mathieu, N. K. Su, S. L. Kristufek, D. J. Lundberg, S. Bhagchandani, I. M. Ghobrial, P. P. Ghoroghchian, J. A. Johnson, *Nat. Nanotechnol.* **2023**, *18*, 184.
[12] X. Li, X. Peng, M. Zoulikha, G. F. Boafo, K. T. Magar, Y. Ju, W. He, *Sig. Transduct. Target. Ther.* **2024**, *9*, 1.
[13] P. Tardi, S. Johnstone, N. Harasyrn, S. W. Xie, T. Harasyrn, N. Zisman, P. Harvie, D. Bermudes, L. Mayer, *Leukemia Res.* **2009**, *33*, 129.
[14] J. E. Lancet, G. L. Uy, J. E. Cortes, L. F. Newell, T. L. Lin, E. K. Ritchie, R. K. Stuart, S. A. Strickland, D. Hogge, S. R. Solomon, R. M. Stone, D. L. Bixby, J. E. Kolitz, G. J. Schiller, M. J. Wieduwilt, D. H. Ryan, A. Hoering, K. Banerjee, M. Chiarella, A. C. Louie, B. C. Medeiros, *J. Clin. Oncol.* **2018**, *36*, 2684.
[15] P. Stelmach, A. Trumpp, *Haematologica* **2023**, *108*, 353.
[16] A. G. X. Zeng, S. Bansal, L. Jin, A. Mitchell, W. C. Chen, H. A. Abbas, M. Chan-Seng-Yue, V. Voisin, P. van Galen, A. Tierens, M. Cheok, C. Preudhomme, H. Dombret, N. Daver, P. A. Futreal, M. D. Minden, J. A. Kennedy, J. C. Y. Wang, J. E. Dick, *Nat. Med.* **2022**, *28*, 1212.
[17] J. Li, H. Wu, Z. Yu, Q. Wang, X. Zeng, W. Qian, S. Lu, L. Jiang, J. Li, M. Zhu, Y. Han, J. Gao, P. Qian, *Nat. Commun.* **2024**, *15*, 5689.
[18] A. Hu, H. Chen, J. Liang, C. Liu, F. Li, C. Mu, *J. Controlled Release* **2021**, *339*, 1.
[19] Y. Huang, Z. Xiao, Z. Guan, Z. Zeng, Y. Shen, X. Xu, C. Zhao, *Acta Pharm. Sin. B* **2020**, *10*, 2384.
[20] J. Ye, J. Jiang, Z. Zhou, Z. Weng, Y. Xu, L. Liu, W. Zhang, Y. Yang, J. Luo, X. Wang, *ACS Nano* **2021**, *15*, 13692.
[21] N. Gong, M. J. Mitchell, *Nat. Nanotechnol.* **2023**, *18*, 548.
[22] S. M. Lawrence, R. Corriden, V. Nizet, *Trends Immunol.* **2020**, *41*, 531.
[23] Z. Luo, Y. Lu, Y. Shi, M. Jiang, X. Shan, X. Li, J. Zhang, B. Qin, X. Liu, X. Guo, J. Huang, Y. Liu, S. Wang, Q. Li, L. Luo, J. You, *Nat. Nanotechnol.* **2023**, *18*, 647.
[24] K. Strebhardt, *Nat. Rev. Drug Discovery* **2010**, *9*, 643.
[25] R. E. A. Gutteridge, M. A. Ndiaye, X. Liu, N. Ahmad, *Mol. Cancer Ther.* **2016**, *15*, 1427.
[26] Z. Yu, P. Deng, Y. Chen, S. Liu, J. Chen, Z. Yang, J. Chen, X. Fan, P. Wang, Z. Cai, Y. Wang, P. Hu, D. Lin, R. Xiao, Y. Zou, Y. Huang, Q. Yu, P. Lan, J. Tan, X. Wu, *Adv. Sci.* **2021**, *8*, 2100759.
[27] J. Du, S. Yue, C. Li, J. Li, S. Zhao, Y. Dong, Y. Zhang, R. Cheng, H. Sun, Z. Zhong, *Nano Today* **2023**, *50*, 101872.
[28] D. E. Discher, F. Ahmed, *Annu. Rev. Biomed. Eng.* **2006**, *8*, 323.
[29] A. C. Wauters, J. F. Scheerstra, M. M. T. van Leent, A. J. P. Teunissen, B. Priem, T. J. Beldman, N. Rother, R. Duivenvoorden, G. Prévot, J. Munitz, Y. C. Toner, J. Deckers, Y. van Elsas, P. Mora-Raimundo, G.

Chen, S. A. Nauta, A. V. D. Verschuur, A. W. Griffioen, D. P. Schrijver, T. Anbergen, Y. Li, H. Wu, A. F. Mason, M. H. M. E. van Stevendaal, E. Kluza, R. A. J. Post, L. A. B. Joosten, M. G. Netea, C. Calcagno, Z. A. Fayad, et al., *Nat. Nanotechnol.* **2024**, *19*, 1735.
[30] D. Shae, K. W. Becker, P. Christov, D. S. Yun, A. K. R. Lytton-Jean, S. Sevimli, M. Ascano, M. Kelley, D. B. Johnson, J. M. Balko, J. T. Wilson, *Nat. Nanotechnol.* **2019**, *14*, 269.
[31] R. Cheng, F. Feng, F. H. Meng, C. Deng, J. Feijen, Z. Y. Zhong, *J. Controlled Release* **2011**, *152*, 2.
[32] A. M. Sofias, T. Lammers, *Nat. Nanotechnol.* **2023**, *18*, 104.
[33] M. Casanova-Acebes, C. Pitaval, L. A. Weiss, C. Nombela-Arrieta, R. Chèvre, N. A-González, Y. Kunisaki, D. Zhang, N. van Rooijen, L. E. Silberstein, C. Weber, T. Nagasawa, P. S. Frenette, A. Castrillo, A. Hidalgo, *Cell* **2013**, *153*, 1025.
[34] J. M. Adrover, A. Aroca-Crevillén, G. Crainiciuc, F. Ostos, Y. Rojas-Vega, A. Rubio-Ponce, C. Cilloniz, E. Bonzón-Kulichenko, E. Calvo, D. Rico, M. A. Moro, C. Weber, I. Lizasoaín, A. Torres, J. Ruiz-Cabello, J. Vázquez, A. Hidalgo, *Nat. Immunol.* **2020**, *21*, 135.
[35] S. B. Coffelt, K. Kersten, C. W. Doornebal, J. Weiden, K. Vrijland, C.-S. Hau, N. J. M. Verstegen, M. Ciampricotti, L. J. A. C. Hawinkels, J. Jonkers, K. E. de Visser, *Nature* **2015**, *522*, 345.
[36] H. Liu, B. Zhang, H. Chen, H. Wang, X. Qin, C. Sun, Z. Pang, Y. Hu, *Adv. Sci.* **2024**, *12*, 2409895.
[37] P. Dhyani, C. Quispe, E. Sharma, A. Bahukhandi, P. Sati, D. C. Attri, A. Szopa, J. Sharifi-Rad, A. O. Docea, I. Mardare, D. Calina, W. C. Cho, *Cancer Cell Int.* **2022**, *22*, 206.
[38] P. E. Czabotar, A. J. Garcia-Saez, *Nat. Rev. Mol. Cell Biol.* **2023**, *24*, 732.
[39] C. Zhang, X. Liu, S. Jin, Y. Chen, R. Guo, *Mol. Cancer* **2022**, *21*, 47.
[40] Y. Wang, X. Wu, Z. Ren, Y. Li, W. Zou, J. Chen, H. Wang, *Drug Resist. Updat.* **2023**, *66*, 100916.
[41] B.-G. Kim, E. Malek, S. H. Choi, J. J. Ignatz-Hoover, J. J. Driscoll, *J. Hematol. Oncol.* **2021**, *14*, 55.
[42] X. Wang, P. J. A. Eichhorn, J. P. Thiery, *Semin. Cancer Biol.* **2023**, *97*, 1.
[43] J. C. Zhao, S. Agarwal, H. Ahmad, K. Amin, J. P. Bewersdorf, A. M. Zeidan, *Blood Rev.* **2022**, *52*, 100905.
[44] A. Khwaja, M. Bjorkholm, R. E. Gale, R. L. Levine, C. T. Jordan, G. Ehninger, C. D. Bloomfield, E. Estey, A. Burnett, J. J. Cornelissen, D. A. Scheinberg, D. Bouscary, D. C. Linch, *Nat. Rev. Dis. Primers* **2016**, *2*, 16010.
[45] G. H. D. Oliveira, L. S. Silva, A. Silva, J. P. A. Lima, V. I. Soares, R. V. Freitas, T. M. Oliveira, D. Silva, V. S. F. Sales, H. D. D. Paiva, R. S. Araujo, A. S. Paiva, G. B. Cavalcanti, A. S. J. Silva, *Blood* **2019**, *134*, 5191.
[46] M. Yamashita, P. V. Dellorusso, O. C. Olson, E. Passegue, *Nat. Rev. Cancer* **2020**, *20*, 365.
[47] D. Vetrie, G. V. Helgason, M. Copland, *Nat. Rev. Cancer* **2020**, *20*, 158.
[48] B. Yuan, S. Ly, N. Khoa, V. Tran, K. Maldonado, C. Kinglsey, J. K. Burks, X. Zhou, B. deCrombrugghe, M. Andreeff, V. L. Battula, *Blood* **2018**, *132*, 86.
[49] N. Yu, Y. Zhang, J. Li, W. Gu, S. Yue, B. Li, F. Meng, H. Sun, R. Haag, J. Yuan, Z. Zhong, *Adv. Mater.* **2021**, *33*, 2007787.